Applied Physics Express

LETTER

Universal linear-optical hyperentangled Bell-state measurement

Applied Physics Express 13, 027004 (2020)
https://doi.org/10.35848/1882-0786/ab67d2

LETTER

Universal linear-optical hyperentangled Bell-state measurement

Cheng-Yan Gao[1,2], Bao-Cang Ren[1*], Yuan-Xia Zhang[2], Qing Ai[2], and Fu-Guo Deng[2,3]

[1]Department of Physics, Capital Normal University, Beijing 100048, People's Republic of China
[2]Department of Physics, Applied Optics Beijing Area Major Laboratory, Beijing Normal University, Beijing 100875, People's Republic of China
[3]NAAM-Research Group, Department of Mathematics, Faculty of Science, King Abdulaziz University, PO Box 80203, Jeddah 21589, Saudi Arabia

*E-mail: renbaocang@cnu.edu.cn

Received November 12, 2019; revised December 17, 2019; accepted January 5, 2020; published online January 21, 2020

Hyperentangled Bell-state measurement (HBSM) is an indispensable building block for implementing high-capacity quantum communication. Here we present a universal HBSM scheme resorting to linear optics, which is efficient to divide 16 hyperentangled Bell states in polarization and momentum degrees of freedom (DOFs) into 14 distinguishable groups assisted by time-bin DOF instead of auxiliary entanglement resource. This HBSM scheme has universal applications in quantum information protocols, such as its applications in the implementation of hyperteleportation and hyperentanglement swapping besides hyperdense coding. It enlarges the efficiency and applicability of linear-optical HBSM in quantum information processing. © 2020 The Japan Society of Applied Physics

Entanglement is a unique phenomenon in quantum mechanics, and it has been extensively applied in many quantum communication protocols, such as quantum key distribution,[1,2] quantum secret sharing,[3] quantum dense coding,[4,5] quantum teleportation,[6] quantum secure direct communication,[7] and so on. Photon system has a wide range of applications in quantum communication, and it owns several degrees of freedom (DOFs), containing polarization, momentum, time-bin,[8] frequency, orbital angular momentum, and so on. Photons can be entangled in multiple DOFs simultaneously, which is referred to hyperentanglement, and it has been demonstrated experimentally in many optical systems.[9–13] Hyperentanglement is an essential quantum correlation in high-capacity quantum communication. The application of hyperentanglement has been widely studied.[14–16] In particular, hyperentanglement can assist the Bell-state analysis (BSA) which is an indispensable part to read out encrypted information. In the conventional BSA scheme, only two of four Bell states can be identified via linear optics.[17–22] After introducing hyperentanglement, i.e. enlarging the Hilbert space, the four Bell states can be identified unambiguously. For example, the four polarization Bell states can be completely differentiated with the help of time-bin or momentum DOF via linear optics, which was firstly proposed by Kwiat and Weinfurter in 1998.[23] Some other improved proposals[9,10,24,25] have also been reported in the past decades.

The channel capacity of quantum communication can be enlarged in a larger Hilbert space. In high-capacity quantum communication, a two-photon system hyperentangled in two DOFs is involved, and the unambiguous differentiation of the 16 orthogonal hyperentangled Bell states is also difficult via linear optics alone.[26] It has been proved that 16 orthogonal hyperentangled Bell states can be classified into 7 groups via linear optics.[26] With the help of giant nonlinear optics in cross-Kerr medium[27] and artificial atom in resonator,[28,29] complete hyperentangled Bell-state analysis (HBSA) schemes have been proposed, which can unambiguously differentiate the 16 orthogonal hyperentangled Bell states with high efficiency in theory. However, it remains a huge challenge to achieve the giant nonlinear interactions of photons in practice. For example, the efficiency of HBSA is 52.2% for the strong coupling regime of quantum-dot spins in micropillar cavities with current experimental parameters,[28] and the efficiency of HBSA is 51.48% for the strong coupling regime of nitrogen-vacancy center in microtoroidal resonator with current experimental parameters.[29] For cross-Kerr medium, the natural cross-Kerr nonlinearities are weak, and the improved Kerr phase shift is small (about 10^{-2}), which could also reduce the efficiency of HBSA.[27,30,31] Instead, if auxiliary quantum resources are introduced, linear-optical HBSA is easy to realize with the current technology. Inspired by the idea of complete BSA, Li and Ghose[32] initially showed that an auxiliary entangled state of additional momentum DOF can be used to assist the analysis of the hyperentangled Bell states for two-photon system in polarization and momentum DOFs in 2017. This scheme can separate the 16 hyperentangled Bell states into 12 groups via linear optics. After introducing additional resources besides auxiliary entangled state, the number of distinguishable hyperentangled Bell states can be increased.[33] However, in these two schemes, the application of linear-optical HBSA is limited to hyperdense coding.

In this letter, we present a universal hyperentangled Bell-state measurement (HBSM) scheme for two-photon system hyperentangled in both polarization and momentum DOFs via linear optics. This scheme can extend the applications of linear-optical HBSM to hyperteleportation and hyperentanglement swapping besides hyperdense coding. In this scheme, the four Bell states ($|\phi_P^{\pm}\rangle_{AB}$ and $|\psi_P^{\pm}\rangle_{AB}$) in the polarization DOF and the four Bell states ($|\phi_S^{\pm}\rangle_{AB}$ and $|\psi_S^{\pm}\rangle_{AB}$) in the momentum DOF can be written as

$$
\begin{aligned}
|\phi_P^{\pm}\rangle_{AB} &= \frac{1}{\sqrt{2}}(|HH\rangle \pm |VV\rangle)_{AB},\\
|\psi_P^{\pm}\rangle_{AB} &= \frac{1}{\sqrt{2}}(|HV\rangle \pm |VH\rangle)_{AB},\\
|\phi_S^{\pm}\rangle_{AB} &= \frac{1}{\sqrt{2}}(|ll\rangle \pm |rr\rangle)_{AB},\\
|\psi_S^{\pm}\rangle_{AB} &= \frac{1}{\sqrt{2}}(|lr\rangle \pm |rl\rangle)_{AB},
\end{aligned}
\tag{1}
$$

where the subscripts P and S denote the polarization DOF and momentum DOF of photons, respectively. The horizontal polarization state is described by $|H\rangle$, and the vertical polarization state is described by $|V\rangle$. The left momentum state is described by $|l\rangle$, and the right momentum state is described by $|r\rangle$. It is easy to see that there are 16

hyperentangled Bell states (i.e. $|\phi_P^{\pm}\rangle_{AB} \otimes |\phi_S^{\pm}\rangle_{AB}$, $|\phi_P^{\pm}\rangle_{AB} \otimes |\psi_S^{\pm}\rangle_{AB}$, $|\psi_P^{\pm}\rangle_{AB} \otimes |\phi_S^{\pm}\rangle_{AB}$, $|\psi_P^{\pm}\rangle_{AB} \otimes |\psi_S^{\pm}\rangle_{AB}$), which have been generated in experiment by Yang et al.[34] To differentiate the 16 hyperentangled Bell states, this scheme introduces two different time-bin modes t_0 and t_1 using the unbalanced interferometer (UI) instead of additional entangled states. Because of the introduction of two time-bin modes, the detectors can be triggered with four types of time intervals (0, t_0, t_1, and $t_1 \pm t_0$). And 16 hyperentangled Bell states can be classified into 14 groups according to the time intervals of detector response together with the detection signatures in Table I.

The setup of universal HBSM is shown in Fig. 1. It consists of linear-optical elements, such as 50:50 beam splitters (BSs), UIs, and polarization beam splitters (PBSs). The UI with two time delays t_0 and t_1 plays a key role in this universal HBSM scheme. The schematic diagram of UI is shown in Fig. 2, which is constituted of PBS, BS, and half-wave plates (HWPs). PBS is used to transmit the horizontal polarization state $|H\rangle$ and reflect the vertical polarization state $|V\rangle$. HWP can perform the Hadamard operation on the polarization mode: $|H\rangle \rightarrow \frac{1}{\sqrt{2}}(|H\rangle + |V\rangle)$ and $|V\rangle \rightarrow \frac{1}{\sqrt{2}}(|H\rangle - |V\rangle)$.

Now let us demonstrate the principle of the universal HBSM by taking the hyperentangled Bell-state $|\phi_P^+\phi_S^-\rangle$ as an example. Here the hyperentangled Bell-state $|\phi_P^+\phi_S^-\rangle$ can be written as

$$|\Psi_1\rangle = \frac{1}{2}(|HH\rangle + |VV\rangle)_{AB} \otimes (|ll\rangle - |rr\rangle)_{AB}. \tag{2}$$

The two photons A and B in the hyperentangled Bell-state $|\phi_P^+\phi_S^-\rangle$ are first sent into the input ports of BSs in Fig. 1. BSs perform the Hadamard operations on the momentum DOF of photons A and B in the following forms

$$\begin{aligned} &|l_A\rangle \rightarrow \frac{1}{\sqrt{2}}(|l_2\rangle + |l_1\rangle), \ |l_B\rangle \rightarrow \frac{1}{\sqrt{2}}(|l_1\rangle - |l_2\rangle), \\ &|r_A\rangle \rightarrow \frac{1}{\sqrt{2}}(|r_2\rangle + |r_1\rangle), \ |r_B\rangle \rightarrow \frac{1}{\sqrt{2}}(|r_1\rangle - |r_2\rangle). \end{aligned} \tag{3}$$

With the effect of BSs, the hyperentangled state of photonic system becomes

$$\begin{aligned} |\Psi_2\rangle = \frac{1}{2\sqrt{2}}&(|HH\rangle + |VV\rangle) \otimes [-|l_2\rangle|l_2\rangle \\ &+ |l_1\rangle|l_1\rangle + |r_2\rangle|r_2\rangle - |r_1\rangle|r_1\rangle]. \end{aligned} \tag{4}$$

Subsequently, the wave packets of two photons are sent into the UI shown in Fig. 2. The wave packets with momentum mode $|l_1\rangle$ or $|l_2\rangle$ will come into UI from the input port l and experience a time delay t_0, while the wave packets with momentum mode $|r_1\rangle$ or $|r_2\rangle$ will directly enter UI from the port r without detention. Afterwards, the wave packets of two photons are transmitted into PBS (shown in Fig. 2). After passing through PBS, the wave packets of photons with momentum mode $|l_1\rangle$ or $|l_2\rangle$ will get longer time delay t_1. Considering the time delays and the operation of PBS, the hyperentangled state $|\Psi_2\rangle$ evolves to

Table I. The relationship between the detection signatures and the hyperentangled Bell states in view of the detection time interval Δt of two photons. G_1, G_2, G_3, and G_4 represent four groups.

	State	Detection signature	Δt
1	$\phi_P^+ \otimes \phi_S^+$	$A_r^+B_l^-$, $A_r^-B_l^+$, $A_l^+B_r^-$, $A_l^-B_r^+$	
2	$\phi_P^- \otimes \phi_S^+$	$A_r^+B_l^+$, $A_r^-B_l^-$, $A_l^+B_r^+$, $A_l^-B_r^-$	0
3	$\phi_P^- \otimes \phi_S^-$	$A_r^+A_r^-$, $A_l^+A_l^-$, $B_r^+B_r^-$, $B_l^+B_l^-$	(G_1)
4	$\phi_P^+ \otimes \phi_S^-$	$A_r^+A_r^+$, $A_r^-A_r^-$, $A_l^+A_l^+$, $A_l^-A_l^-$	
		$B_r^+B_r^+$, $B_r^-B_r^-$, $B_l^+B_l^+$, $B_l^-B_l^-$	
5	$\psi_P^+ \otimes \psi_S^-$	$A_r^+A_r^+$, $A_r^-A_r^-$, $A_l^+A_l^+$, $A_l^-A_l^-$	
		$B_r^+B_r^+$, $B_r^-B_r^-$, $B_l^+B_l^+$, $B_l^-B_l^-$	
		$A_r^+B_l^-$, $A_r^-B_l^+$, $A_l^+B_r^-$, $A_l^-B_r^+$	
6	$\psi_P^+ \otimes \psi_S^+$	$A_r^+A_l^-$, $A_r^-A_l^+$, $B_r^+B_l^-$, $B_r^-B_l^+$	
		$A_r^+B_r^+$, $A_r^-B_r^-$, $A_l^+B_l^+$, $A_l^-B_l^-$	t_0
7	$\psi_P^- \otimes \psi_S^+$	$A_r^+A_r^-$, $A_l^+A_l^-$, $B_r^+B_r^-$, $B_l^+B_l^-$	(G_2)
		$A_r^+B_l^+$, $A_r^-B_l^-$, $A_l^+B_r^+$, $A_l^-B_r^-$	
8	$\psi_P^- \otimes \psi_S^-$	$A_r^+A_l^+$, $A_r^-A_l^-$, $B_r^+B_l^+$, $B_r^-B_l^-$	
		$A_r^+B_r^-$, $A_r^-B_r^+$, $A_l^+B_l^-$, $A_l^-B_l^+$	
9	$\psi_P^+ \otimes \phi_S^-$	$A_r^+A_r^+$, $A_r^-A_r^-$, $A_l^+A_l^+$, $A_l^-A_l^-$	
		$B_r^+B_r^+$, $B_r^-B_r^-$, $B_l^+B_l^+$, $B_l^-B_l^-$	
		$A_r^+B_l^+$, $A_r^-B_l^-$, $A_l^+B_r^+$, $A_l^-B_r^-$	
10	$\psi_P^+ \otimes \phi_S^+$	$A_r^+A_r^-$, $A_l^+A_l^-$, $B_r^+B_r^-$, $B_l^+B_l^-$	
		$A_r^+B_l^-$, $A_r^-B_l^+$, $A_l^+B_r^-$, $A_l^-B_r^+$	t_1
11	$\psi_P^- \otimes \phi_S^+$	$A_r^+A_l^+$, $A_r^-A_l^-$, $B_r^+B_l^+$, $B_r^-B_l^-$	(G_3)
		$A_r^+B_r^+$, $A_r^-B_r^-$, $A_l^+B_l^+$, $A_l^-B_l^-$	
12	$\psi_P^- \otimes \phi_S^-$	$A_r^+A_l^-$, $A_r^-A_l^+$, $B_r^+B_l^-$, $B_r^-B_l^+$	
		$A_r^+B_r^-$, $A_r^-B_r^+$, $A_l^+B_l^-$, $A_l^-B_l^+$	
13		$A_r^+A_r^+$, $A_r^-A_r^-$, $A_r^+A_r^-$, $A_l^+A_l^+$	
	$\phi_P^+ \otimes \psi_S^-$	$A_l^-A_l^-$, $A_l^+A_l^-$, $B_r^+B_r^+$, $B_r^-B_r^-$	
	$\phi_P^- \otimes \psi_S^-$	$B_r^+B_r^-$, $B_l^+B_l^+$, $B_l^-B_l^-$, $B_l^+B_l^-$	
		$A_r^+B_l^+$, $A_r^-B_l^-$, $A_r^+B_l^-$, $A_r^-B_l^+$	
		$A_l^+B_r^+$, $A_l^-B_r^-$, $A_l^+B_r^-$, $A_l^-B_r^+$	$t_1 \pm t_0$
14		$A_r^+A_l^+$, $A_r^-A_l^-$, $A_r^+A_l^-$, $A_r^-A_l^+$	(G_4)
	$\phi_P^+ \otimes \psi_S^+$	$B_r^+B_l^+$, $B_r^-B_l^-$, $B_r^+B_l^-$, $B_r^-B_l^+$	
	$\phi_P^- \otimes \psi_S^+$	$A_r^+B_r^+$, $A_r^-B_r^-$, $A_r^+B_r^-$, $A_r^-B_r^+$	
		$A_l^+B_l^+$, $A_l^-B_l^-$, $A_l^+B_l^-$, $A_l^-B_l^+$	

$$\begin{aligned} |\Psi_3\rangle = \frac{1}{2\sqrt{2}}\{&|HH\rangle[-D(t_0+t_1)|l_2\rangle D(t_0+t_1)|l_2\rangle \\ &+ D(t_0+t_1)|l_1\rangle D(t_0+t_1)|l_1\rangle \\ &+ I|r_2\rangle I|r_2\rangle - I|r_1\rangle I|r_1\rangle] + |VV\rangle[-D(t_0)|r_1\rangle D(t_0)|r_1\rangle \\ &+ D(t_0)|r_2\rangle D(t_0)|r_2\rangle + D(t_1)|l_1\rangle D(t_1)|l_1\rangle \\ &- D(t_1)|l_2\rangle D(t_1)|l_2\rangle]\}. \end{aligned} \tag{5}$$

Here I, $D(t_0)$, $D(t_1)$, and $D(t_0+t_1)$ are linear time delay operators performed on the photons,[35] which satisfy the following relations:

$$I = D(0), \quad D(t_0+t_1) = D(t_0)D(t_1). \tag{6}$$

In the following, the wave packets of two photons are superposed on BSs which convert the momentum modes of photons as

$$\begin{aligned} &|l_1\rangle \rightarrow \frac{1}{\sqrt{2}}(|\tilde{r}_2\rangle + |\tilde{l}_1\rangle), \ |l_2\rangle \rightarrow \frac{1}{\sqrt{2}}(|\tilde{r}_1\rangle + |\tilde{l}_2\rangle), \\ &|r_1\rangle \rightarrow \frac{1}{\sqrt{2}}(|\tilde{l}_2\rangle - |\tilde{r}_1\rangle), \ |r_2\rangle \rightarrow \frac{1}{\sqrt{2}}(|\tilde{l}_1\rangle - |\tilde{r}_2\rangle). \end{aligned} \tag{7}$$

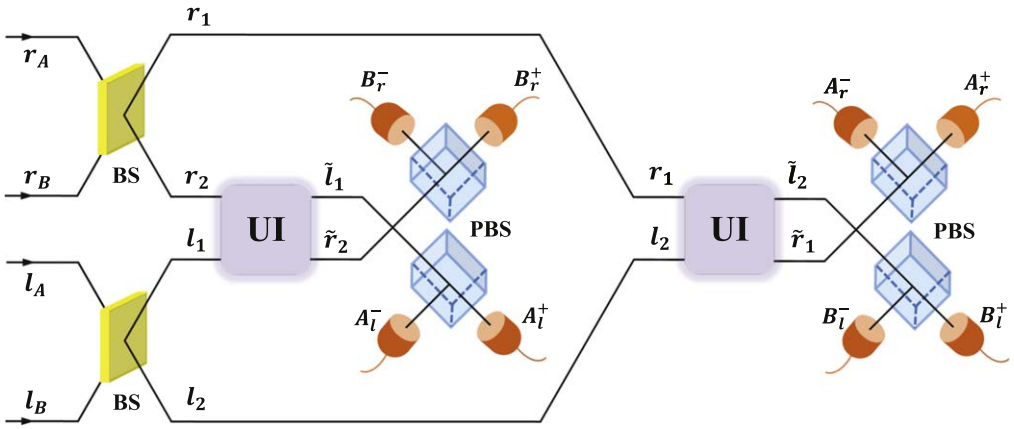

Fig. 1. (Color online) Schematic diagram for the universal hyperentangled Bell-state measurement (HBSM). Here UI represents the unbalanced interferometer in Fig. 2. BS is 50:50 beam splitter. PBS is polarization beam splitter.

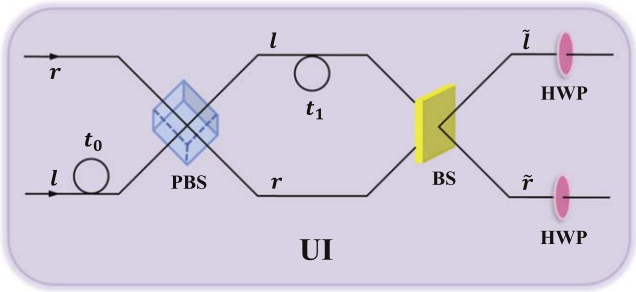

Fig. 2. (Color online) Schematic diagram for unbalanced interferometer (UI). HWP represents half-wave plate. The optical circle on the path l denotes time delay t_0 or t_1.

After two photons pass through BSs, HWPs perform the polarization Hadamard operations on the wave packets of two photons. During the operations of HWPs, the wave packets with the identical modes in both the polarization DOF and momentum DOF can interfere with each other under the constructive-interfere condition, i.e. $\omega t_0 = 2n\pi$ and $\omega t_1 = 2m\pi$ (n and m are integers, and ω is the frequency of input photon).[25] After the interaction of the wave packets, the hyperentangled state $|\Psi_3\rangle$ evolves as

$$\begin{aligned}|\Psi_4\rangle = \frac{1}{4\sqrt{2}}(|H\rangle|H\rangle + |V\rangle|V\rangle)\sum_{i=0}^{i=3}(-D(\tau_i)|\tilde{r}_1\rangle D(\tau_i)|\tilde{r}_1\rangle \\ - D(\tau_i)|\tilde{l}_2\rangle D(\tau_i)|\tilde{l}_2\rangle \\ + D(\tau_i)|\tilde{r}_2\rangle D(\tau_i)|\tilde{r}_2\rangle + D(\tau_i)|\tilde{l}_1\rangle D(\tau_i)|\tilde{l}_1\rangle).\end{aligned} \tag{8}$$

Here $\tau_0 = 0$, $\tau_1 = t_0$, $\tau_2 = t_1$, and $\tau_3 = t_0 + t_1$. If the time resolution of detector is 4 ns, the time delays t_0 and t_1 in UI could be set to 5 ns and 10 ns in experiment, respectively.[25]

At the output ports of UI, the two photons are projected to the polarization basis $\{|H\rangle, |V\rangle\}$ by PBSs and detected by photon detectors. The detection signatures of the hyperentangled Bell-state $|\phi_P^+\phi_S^-\rangle$ are

$$\begin{aligned}&\{A_r^+A_r^+, A_r^-A_r^-, A_l^+A_l^+, A_l^-A_l^-, \\ &B_r^+B_r^+, B_r^-B_r^-, B_l^+B_l^+, B_l^-B_l^-\}.\end{aligned} \tag{9}$$

Here the superscript "+" ("−") indicates that photon is transmitted (reflected) by PBS at the output port. Obviously, "$A_r^+A_r^+$" represents that two photons are routed to one output port and trigger one detector A_r^+ at the same time. This requires photon number resolving detector, which has been resolved by Schuck et al.[9]

So far, we have completed all the steps of universal HBSM for the hyperentangled Bell-state $|\phi_P^+\phi_S^-\rangle$. The other 15 hyperentangled Bell states can also be measured with the same method. We list the detection signatures of the 16 hyperentangled Bell states in Table I, in which the 16 hyperentangled Bell states are classified into four groups (G_1, G_2, G_3, G_4) according to four types of detection time intervals (0, t_0, t_1, $t_1 \pm t_0$). Each group contains four states. In the groups G_1, G_2, and G_3, the detection signatures of four hyperentangled Bell states are different from each other. In the fourth group G_4, two hyperentangled Bell states $|\phi_P^+\psi_S^+\rangle$ and $|\phi_P^-\psi_S^+\rangle$ ($|\phi_P^+\psi_S^-\rangle$ and $|\phi_P^-\psi_S^-\rangle$) have the same detection signatures. This is equivalent to dividing the 16 hyperentangled Bell states into 14 groups. Therefore, our scheme is efficient compared with the previous HBSA scheme which forms 12 distinguishable groups resorting to auxiliary entangled state and linear optics.[32]

The universal linear-optical HBSM scheme is a useful tool in quantum communication. Here we use this universal HBSM scheme to teleport a two-DOF quantum state from Alice to her distant communication party Bob, which is shown in Fig. 3. At the beginning, Alice has one single photon A, and Alice and Bob share one pair of hyperentangled photons BC. Photon A is in a polarization-momentum state $|\Phi\rangle_A$ which can be written as

$$|\Phi\rangle_A = (\alpha|H\rangle + \beta|V\rangle)_A \otimes (\gamma|r\rangle + \delta|l\rangle)_A. \tag{10}$$

Here $|\alpha|^2 + |\beta|^2 = |\gamma|^2 + |\delta|^2 = 1$. Photon pair BC is in a polarization-momentum hyperentangled Bell-state $|\phi_P^+\phi_S^+\rangle_{BC}$. Alice sends photon A and photon B into the universal HBSM setup in Fig. 1. After HBSM process, the detection signature

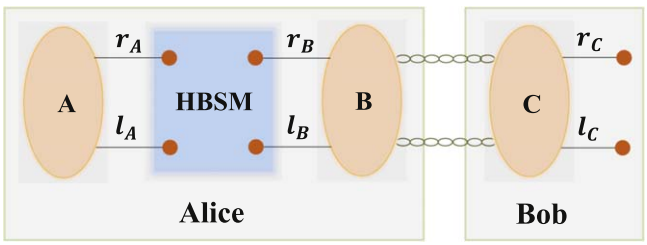

Fig. 3. (Color online) Schematic diagram for the hyperteleportation with the help of universal HBSM in Fig. 1.

of photons AB corresponds to one of 14 groups in Table I, and photon C is collapsed into a two-DOF state. For example, if the detection signature signifies that the state of photons AB is $|\psi_P^-\psi_S^-\rangle_{AB}$, we can infer photon C is collapsed into the following state

$$|\Phi\rangle_C = {}_{AB}\langle\psi_P^-\psi_S^-|\Phi\rangle_A|\phi_P^+\phi_S^+\rangle_{BC} = (\alpha|V\rangle - \beta|H\rangle)_C \otimes (-\gamma|l\rangle + \delta|r\rangle)_C. \quad (11)$$

After bit-flip and phase-flip operations are performed on both the polarization and momentum DOFs of photon C, the state $|\Phi\rangle_A$ is transferred to photon C completely. In particular, when the detection signature of photons AB corresponds to the fourth group G_4 in Table I, only the momentum state of photon C is identified, while the polarization state of photon C can not be identified. So the efficiency of this hyperteleportation is 87.5%. In the same way, the universal HBSM scheme can be used to realize hyperentanglement swapping, hyperdense coding, and so on.

In summary, we have presented a universal linear-optical HBSM scheme only assisted by time-bin DOF, which has enlarged the efficiency and applicability of linear-optical HBSM. This universal linear-optical HBSM scheme has three outstanding advantages. Firstly, the scheme has universal applications in quantum information processing, which is suitable for implementing not only hyperdense coding but also hyperentanglement swapping and hyperteleportation, as time-bin DOF is easy to introduce and control in the HBSM process. Secondly, this universal HBSM scheme is efficient compared with the HBSA scheme using auxiliary entanglement. With the help of time-bin DOF, the HBSM scheme divides the 16 hyperentangled Bell states into 14 groups, while the 16 hyperentangled Bell states can be divided into 12 groups using auxiliary entanglement.[32] For example, when applying the universal HBSM scheme into hyperdense coding, $\log_2^{14} \approx 3.81$ bits/photon information can be transmitted, which is better than the proposal with auxiliary entanglement[32] ($\log_2^{12} \approx 3.58$ bits/photon). Thirdly, the scheme relies on linear-optical elements, which reduces the difficulty and the resource consumption in practice. Therefore, our universal linear-optical HBSM scheme has potential applications in high-capacity quantum communication.

Acknowledgments This work was supported by the National Natural Science Foundation of China under Grant Numbers 11604226, 11674033, 11474026, and 11505007, and the Science and Technology Program Foundation of the Beijing Municipal Commission of Education of China under Grant Numbers KM201710028005 and CIT&TCD201904080.

ORCID iDs Bao-Cang Ren https://orcid.org/0000-0002-7679-3612

1) A. K. Ekert, Phys. Rev. Lett. **67**, 661 (1991).
2) C. H. Bennett, G. Brassard, and N. D. Mermin, Phys. Rev. Lett. **68**, 557 (1992).
3) M. Hillery, V. Bužek, and A. Berthiaume, Phys. Rev. A **59**, 1829 (1999).
4) C. H. Bennett and S. J. Wiesner, Phys. Rev. Lett. **69**, 2881 (1992).
5) X. S. Liu, G. L. Long, D. M. Tong, and L. Feng, Phys. Rev. A **65**, 022304 (2002).
6) C. H. Bennett, G. Brassard, C. Crepeau, R. Jozsa, A. Peres, and W. K. Wootters, Phys. Rev. Lett. **70**, 1895 (1993).
7) G. L. Long and X. S. Liu, Phys. Rev. A **65**, 032302 (2002).
8) H.-P. Lo, T. Ikuta, N. Matsuda, T. Honjo, and H. Takesue, Appl. Phys. Express **11**, 092801 (2018).
9) C. Schuck, G. Huber, C. Kurtsiefer, and H. Weinfurter, Phys. Rev. Lett. **96**, 190501 (2006).
10) M. Barbieri, G. Vallone, P. Mataloni, and F. De Martini, Phys. Rev. A **75**, 042317 (2007).
11) G. Vallone, R. Ceccarelli, F. De Martini, and P. Mataloni, Phys. Rev. A **79**, 030301(R) (2009).
12) M. Barbieri, C. Cinelli, P. Mataloni, and F. De Martini, Phys. Rev. A **72**, 052110 (2005).
13) C. Barreiro, N. K. Langford, N. A. Peters, and P. G. Kwiat, Phys. Rev. Lett. **95**, 260501 (2005).
14) X. L. Wang, X. D. Cai, Z. E. Su, M. C. Chen, D. Wu, L. Li, N. L. Liu, C. Y. Lu, and J. W. Pan, Nature **518**, 516 (2015).
15) T. J. Wang, C. Cao, and C. Wang, Phys. Rev. A **89**, 052303 (2015).
16) T. Li and G. L. Long, Phys. Rev. A **94**, 022343 (2016).
17) L. Vaidman and N. Yoran, Phys. Rev. A **59**, 116 (1999).
18) N. Lütkenhaus, J. Calsamiglia, and K.-A. Suominen, Phys. Rev. A **59**, 3295 (1999).
19) J. Calsamiglia, Phys. Rev. A **65**, 030301(R) (2002).
20) K. Mattle, H. Weinfurter, P. G. Kwiat, and A. Zeilinger, Phys. Rev. Lett. **76**, 4656 (1996).
21) J. A. W. van Houwelingen, N. Brunner, A. Beveratos, H. Zbinden, and N. Gisin, Phys. Rev. Lett. **96**, 130502 (2006).
22) R. Ursin, T. Jennewein, M. Aspelmeyer, R. Kaltenbaek, M. Lindenthal, P. Walther, and A. Zeilinger, Nature **430**, 849 (2004).
23) P. G. Kwiat and H. Weinfurter, Phys. Rev. A **58**, 2623(R) (1998).
24) S. P. Walborn, S. Padua, and C. H. Monken, Phys. Rev. A **68**, 042313 (2003).
25) B. P. Williams, R. J. Sadlier, and T. S. Humble, Phys. Rev. Lett. **118**, 050501 (2017).
26) T. C. Wei, J. T. Barreiro, and P. G. Kwiat, Phys. Rev. A **75**, 060305 (2007).
27) Y. B. Sheng, F. G. Deng, and G. L. Long, Phys. Rev. A **82**, 032318 (2010).
28) T. J. Wang, Y. Lu, and G. L. Long, Phys. Rev. A **86**, 042337 (2012).
29) Q. Liu and M. Zhang, Phys. Rev. A **91**, 062321 (2015).
30) X. H. Li and S. Ghose, Phys. Rev. A **93**, 022302 (2016).
31) Y. B. Sheng and L. Zhou, Sci. Rep. **5**, 13453 (2015).
32) X. H. Li and S. Ghose, Phys. Rev. A **96**, 020303(R) (2017).
33) C. Y. Gao, B. C. Ren, Y. X. Zhang, Q. Ai, and F. G. Deng, Ann. Phys. (Berlin) **531**, 1900201 (2019).
34) T. Yang, Q. Zhang, J. Zhang, J. Yin, Z. Zhao, M. Zukowski, Z. B. Chen, and J. W. Pan, Phys. Rev. Lett. **95**, 240406 (2005).
35) T. Li, G. Y. Wang, F. G. Deng, and G. L. Long, Sci. Rep. **6**, 20677 (2016).